ACS APPLIED MATERIALS & INTERFACES

Research Article

www.acsami.org

Highly Branched RuO_2 Nanoneedles on Electrospun TiO_2 Nanofibers as an Efficient Electrocatalytic Platform

Su-jin Kim,[†,∥] Yu Kyung Cho,[†,∥] Jeesoo Seok,[†] Nam-Suk Lee,[‡] Byungrak Son,[§] Jae Won Lee,[⊥] Jeong Min Baik,[⊥] Chongmok Lee,[†] Youngmi Lee,*[,†] and Myung Hwa Kim*[,†]

[†]Department of Chemistry & Nano Science, Ewha Womans University, Seoul 120-750, Korea

[‡]National Institute for Nanomaterials Technology (NINT), Pohang University of Science and Technology (POSTECH), Pohang 790-784, Korea

[§]Robotic Research Division, Daegu Gyeongbok Institute of Science & Technology (DGIST), Dalseong 711-873, Korea

[⊥]School of Mechanical and Advanced Materials Engineering, KIST-UNIST-Ulsan Center for Convergent Materials, Ulsan National Institute of Science and Technology (UNIST), Ulsan 689-798, South Korea

Supporting Information

ABSTRACT: Highly single-crystalline ruthenium dioxide (RuO_2) nanoneedles were successfully grown on polycrystalline electrospun titanium dioxide (TiO_2) nanofibers for the first time by a combination of thermal annealing and electrospinning from RuO_2 and TiO_2 precursors. Single-crystalline RuO_2 nanoneedles with relatively small dimensions and a high density on electrospun TiO_2 nanofibers are the key feature. The general electrochemical activities of RuO_2 nanoneedles−TiO_2 nanofibers and $Ru(OH)_3$-TiO_2 nanofibers toward the reduction of $[Fe(CN)_6]^{3-}$ were carefully examined by cyclic voltammetry carried out at various scan rates; the results indicated favorable charge-transfer kinetics of $[Fe(CN)_6]^{3-}$ reduction via a diffusion-controlled process. Additionally, a test of the analytical performance of the RuO_2 nanoneedles−TiO_2 nanofibers for the detection of a biologically important molecule, hydrogen peroxide (H_2O_2), indicated a high sensitivity (390.1 ± 14.9 $\mu A\ mM^{-1}\ cm^{-2}$ for H_2O_2 oxidation and 53.8 ± 1.07 $\mu A\ mM^{-1}\ cm^{-2}$ for the reduction), a low detection limit (1 μM), and a wide linear range (1−1000 μM), indicating H_2O_2 detection performance better than or comparable to that of other sensing systems.

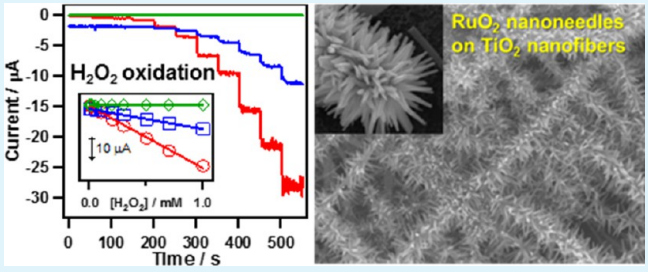

KEYWORDS: *ruthenium oxide, titanium oxide, nanoneedle, nanofiber, electrocatalyst, H_2O_2 electrochemical reaction*

INTRODUCTION

Transition metal oxides exhibit excellent electrochemical properties with many interesting applications. Among these oxides, ruthenium dioxide (RuO_2) is of considerable interest as a candidate for use in electrodes in various applications because of its high catalytic activity, low resistivity, and superior chemical and thermal stability.[1,2] Because RuO_2 is known to be one of the best redox electrochemical capacitor electrode materials, most research on RuO_2 nanocomposites has focused on the development of supercapacitors.[2,3] The electrocatalytic applications of RuO_2 have been reviewed elsewhere. In contrast, the literature contains only a few reports on the use of RuO_2 as an electrode material for the oxidative detection of biological species such as insulin,[4] dopamine,[5] and nitric oxide (NO).[6] Recently, we reported the facile growth of one-dimensional RuO_2 nanostructures in high density on a single carbon fiber (CF) via a simple thermal annealing process of a ruthenium hydroxide ($Ru(OH)_3$) precursor.[7,8] The feasibility of the prepared RuO_2 nanorods-CF for use as a microsensing element with high sensitivity was confirmed for the electrochemical oxidation of hydrogen peroxide (H_2O_2)[7] and NO.[8]

Titanium dioxide (TiO_2) has been extensively studied for use in many applications, including environmental catalysts, biomaterials, photocatalysts, and solar cells, because of its low cost and unique physicochemical properties, which include high photocatalytic activity, environmentally benign characteristics, high reflective index, noncorrosion, good stability, and a wide band gap.[9−12] In particular, TiO_2 nanostructures have recently garnered significant interest in the field of water-splitting hydrogen generation for future cost-effective energy production. Among the preparation methods of well-defined one-dimensional TiO_2 nanostructures, the electrospinning process has recently been widely recognized as a very practical technique that can be used to easily synthesize one-dimensional nanostructures such as nanofibers at low cost.[13−15] The electrospun nanofibers exhibit a very large surface-area-to-volume ratio and an additional advantage of being able to form complexes with other materials. Because of these characteristics

Received: April 13, 2015
Accepted: July 2, 2015
Published: July 2, 2015

DOI: 10.1021/acsami.5b03178
ACS Appl. Mater. Interfaces 2015, 7, 15321−15330

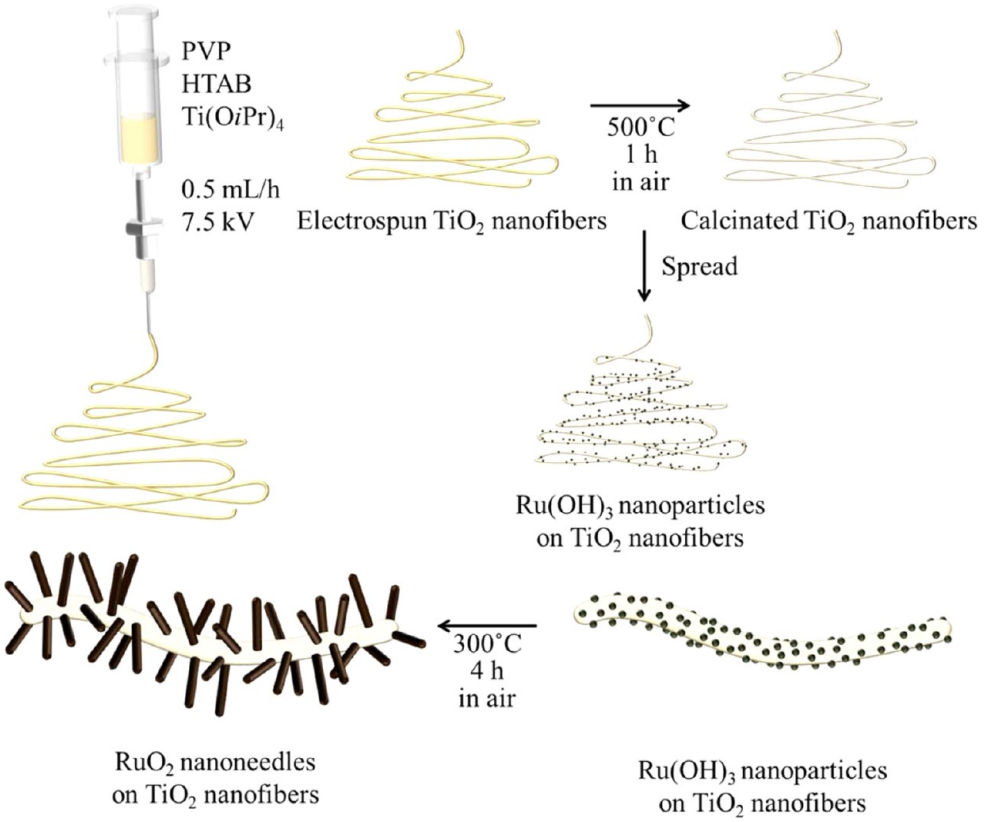

Figure 1. Schematic illustration of the growth process for single crystalline RuO_2 nanoneedles on electrospun TiO_2 nanofibers.

of the nanofibers, they have been applied in various chemical and biological sensors; filters; medical, environmental, energy, and electric materials; and electric devices. They have also been used as catalysts and reinforcing materials.[16]

In this study, we have focused on obtaining, for the first time, hybrid nanoarchitectures of highly branched RuO_2 nanoneedles directly grown on electrospun TiO_2 nanofibers; these nanoarchitectures exhibit efficient electrocatalytic performance for electrochemical sensing applications. The combination of RuO_2 and TiO_2 in one-dimensional nanostructures could lead to synergistic catalytic effects and represent a cost-effective synthetic approach because of the relatively lower loading of expensive RuO_2 onto the TiO_2 nanofibers. Polycrystalline TiO_2 nanofibers that serve as a backbone were first readily prepared from a titanium isopropoxide precursor solution by the electrospinning process; single-crystalline RuO_2 nanoneedles were then grown on the surface of electrospun TiO_2 nanofibers by a low-temperature thermal annealing process of a $Ru(OH)_3$ precursor solution. Figure 1 clearly represents the schematic illustration of the growth process for single crystalline RuO_2 nanoneedles on electrospun TiO_2 nanofibers as we propose in this study. We then explored the fundamental electrochemical performance of the system as an effective electrode material to examine the feasibility of the application of this approach to real systems. Finally, we investigated the use of an electrode based on RuO_2 nanoneedles and TiO_2 nanofibers as a low-cost and highly efficient electrochemical sensing element for H_2O_2 molecules in biological systems. The H_2O_2 molecules in biological systems are byproducts of oxidase enzyme activity and are also involved in many types of biological processes, such as aging and cancer, because of their *in vivo* generation by superoxide radicals.

EXPERIMENTAL SECTION

Growth of electrospun TiO_2 nanofibers. To prepare the precursor solution, 0.2 g of polyvinylpyrrolidone (PVP, Mw = 1,300,000, Sigma-Aldrich) and 0.01 g of hexadecyltrimethylammonium bromide (HTAB, Sigma-Aldrich) were dissolved in 2.3 mL of ethanol by stirring. Five hundred milligrams of titanium isopropoxide ($Ti(OCH(CH_3)_2)_4$, 98%. Sigma-Aldrich) was dissolved in a mixed solvent of 1 mL of ethanol and 1 mL of acetic acid for 10 min; this solution was then added to the polymer solution. After being stirred for 3 h, the precursor solution was drawn into a syringe and displaced to the needle tip of an electrospinning system (NanoNC ESR200R2) at a flow rate of 0.5 mL/h; the distance between the tip of the needle and the grounded aluminum plate was approximately 10 cm. The needle was connected to a high-voltage power source, and a voltage of 7.5 kV was applied. The gauge of the plastic disposable needle was 27 as a syringe needle. The electrospun TiO_2/polymer nanofibers were dried at 60 °C in an oven for 1 day and then calcined at 500 °C for 1 h in air. After the calcination process, TiO_2 nanofibers were obtained.

Growth of RuO_2 nanoneedles on electrospun TiO_2 nanofibers. The ruthenium hydroxide precursor was synthesized through a simple reaction of 10 mM ruthenium chloride hydrate ($RuCl_3 \bullet xH_2O$, Sigma-Aldrich, 99.98%) and a dilute NaOH solution.[17] A 10 mM $RuCl_3 \bullet xH_2O$ solution was first prepared in acidic solution at pH 2.3. The dilute NaOH solution was dropped into the $RuCl_3 \bullet xH_2O$ solution until the pH was approximately 10.00; a $Ru(OH)_3$ solution was then obtained in the form of suspended particles. After the precursor solution was stirred for 1 h, it was rinsed 5 times with distilled water. The $Ru(OH)_3$ particles were then redispersed in pure distilled water. The $Ru(OH)_3$ precursor was dropped directly onto the TiO_2 nanofibers on a Si wafer (001) substrate. After drying for 30 min, the sample was placed at the center of the furnace at 300 °C for 4 h in air. The furnace was then allowed to cool to room temperature in air. Finally, RuO_2 nanoneedles successfully grown on the electrospun TiO_2 nanofibers were obtained. For comparison, TiO_2 nanofibers loaded with ruthenium hydroxide were also synthesized ($Ru(OH)_3$-TiO_2

DOI: 10.1021/acsami.5b03178
ACS Appl. Mater. Interfaces 2015, 7, 15321−15330

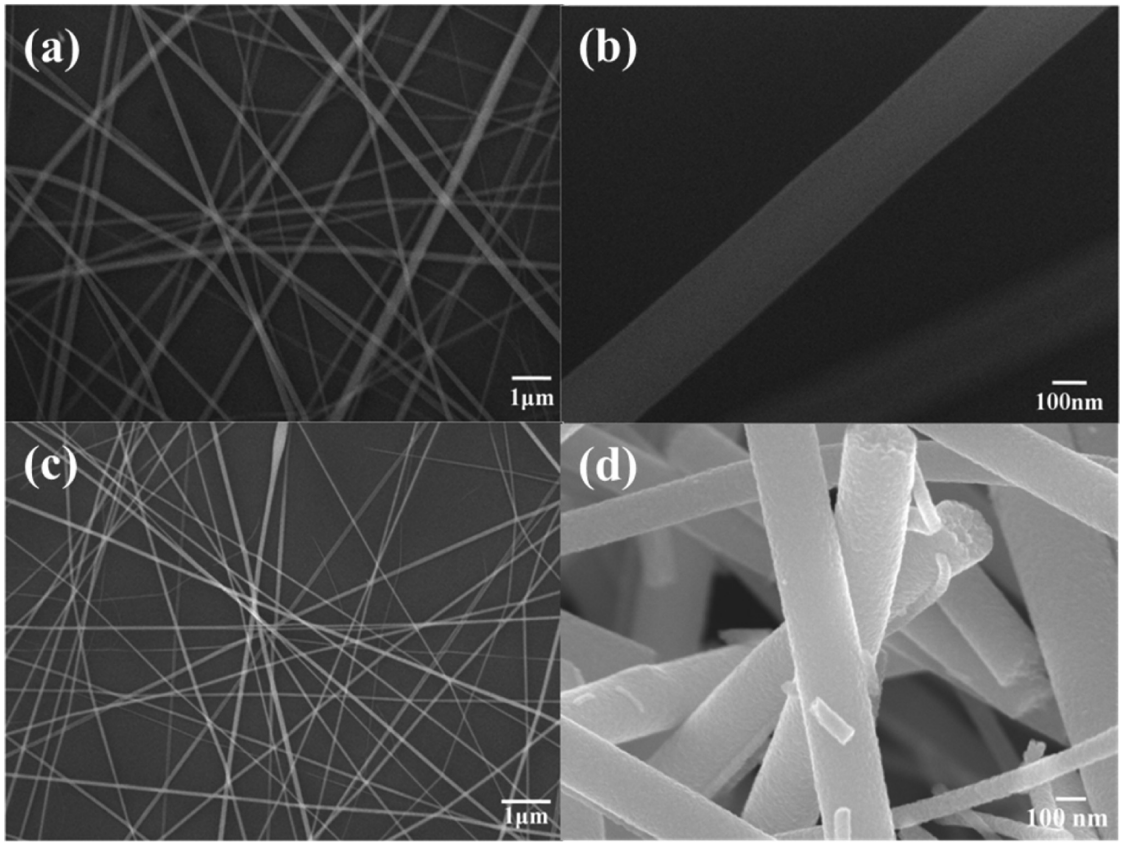

Figure 2. SEM images of electrospun TiO_2 nanofibers: (a) and (b) are precalcined TiO_2 nanofibers; (c) and (d) are TiO_2 nanofibers postcalcined at 500 °C for 4 h.

nanofibers). The synthetic process was the same as that for the growth of RuO_2 nanoneedles, but the growth temperature was 100 °C for 10 min. Finally, the products were characterized by scanning electron microscopy (SEM), X-ray diffraction (XRD) and high-resolution transmission electron microscopy (HR-TEM, Cs-corrected STEM, JEM-2100F).

Electrodes and electrochemical measurements. All electrochemical measurements were performed with a CHI 920C workstation (CH Instruments) and a RDE-1 rotor/Epsilon electrochemical analyzer (BAS Instruments) in a Faraday cage using a three-electrode cell to reduce noise. A saturated calomel electrode (SCE), a coiled platinum wire, and a modified glassy carbon (GC) disk electrode (disk diameter =3 mm, Bioanalytical Systems, Inc.) were used as the reference electrode, the counter electrode, and the working electrode, respectively. Prior to the electrode surface modification, a GC electrode was wet-polished on a polishing cloth using a 3-μm alumina slurry, rinsed with distilled water, and finally sonicated in deionized water for 5 min to remove the residual alumina slurry from the electrode surface.

Ten milligrams of each material (electrospun TiO_2 nanofibers, $Ru(OH)_3$-TiO_2 nanofibers or RuO_2 nanoneedles−TiO_2 nanofibers) was suspended in 5.00 mL of deionized water (2 mg mL^{-1}). Six microliters of the suspended RuO_2 nanowires−TiO_2 nanofibers solution (or $Ru(OH)_3$-TiO_2 nanofibers or TiO_2 nanofibers) was pipetted onto the cleaned GC disk electrode surface and then allowed to dry in an oven at 60 °C for 10 min. These loading and drying steps were repeated five times to load a total of 60 μg of the RuO_2 nanoneedles−TiO_2 nanofibers suspension (or $Ru(OH)_3$-TiO_2 nanofibers or TiO_2 nanofibers). Afterward, 10 μL of 0.05 wt % Nafion solution was applied to the electrode to securely adhere the RuO_2 nanoneedles−TiO_2 nanofibers (or $Ru(OH)_3$-TiO_2 nanofibers or TiO_2 nanofibers).

Cyclic voltammetry (CV) was conducted using GC electrodes loaded with RuO_2 nanoneedles−TiO_2 nanofibers, $Ru(OH)_3$-TiO_2 nanofibers or TiO_2 nanofibers. The potential scans were performed at various rates (1, 2, 5, 10, 20, 50, 100, and 150 mV s^{-1}) with the electrodes immersed in a solution containing 10 mM $[Fe(CN)_6]^{3-}$ and 1.0 M KCl or in a solution containing 1.0 M KCl. Electrochemical impedance spectroscopy (EIS) was performed in a solution containing 10 mM $[Fe(CN)_6]^{3-}$ at 0.139 V (vs SCE) in the frequency range from 1 Hz to 10 kHz.

Rotating disk electrode (RDE) voltammetry was carried out using GC electrodes loaded with RuO_2 nanoneedles−TiO_2 nanofibers (or $Ru(OH)_3$-TiO_2 nanofibers or TiO_2 nanofibers). The experiments were performed at a rotation rate of 100 rpm and at a scan rate of 5 mV s^{-1}, with the electrodes immersed in 0.05 M phosphate buffer saline (PBS, pH 7.4) solution containing 5 mM H_2O_2. The amperometric responses of these electrodes to the varying H_2O_2 concentration were measured in magnetically stirred 0.05 M PBS solution (pH 7.4). Prior to the amperometric measurements, each electrode was prepolarized at 0.6 V (vs SCE) for H_2O_2 oxidation or at 0.0 V (vs SCE) for H_2O_2 reduction for 30 min while immersed in 0.05 M PBS (pH 7.4). The H_2O_2 standard solution was prepared daily using PBS solution and was stored at 4 °C before use. Potassium ferricyanide ($K_3[Fe(CN)_6]$), potassium chloride (KCl), sodium phosphate monobasic (NaH_2PO_4), sodium phosphate dibasic (Na_2HPO_4), H_2O_2 (35 wt % solution in water) and Nafion perfluorinated ion-exchange resin (5.0 wt % solution) were purchased from Sigma-Aldrich (St. Louis, USA). All other chemicals used were of analytical grade, and all solutions were prepared with deionized water (resistivity ≥18 MΩ cm).

RESULTS AND DISCUSSION

RuO_2 nanoneedles on electrospun TiO_2 nanofibers. Figure 2 presents SEM images of electrospun TiO_2 nanofibers synthesized from a titanium tetraisopropoxide and PVP mixed precursor solution by the electrospinning process. The titanium

DOI: 10.1021/acsami.5b03178
ACS Appl. Mater. Interfaces 2015, 7, 15321−15330

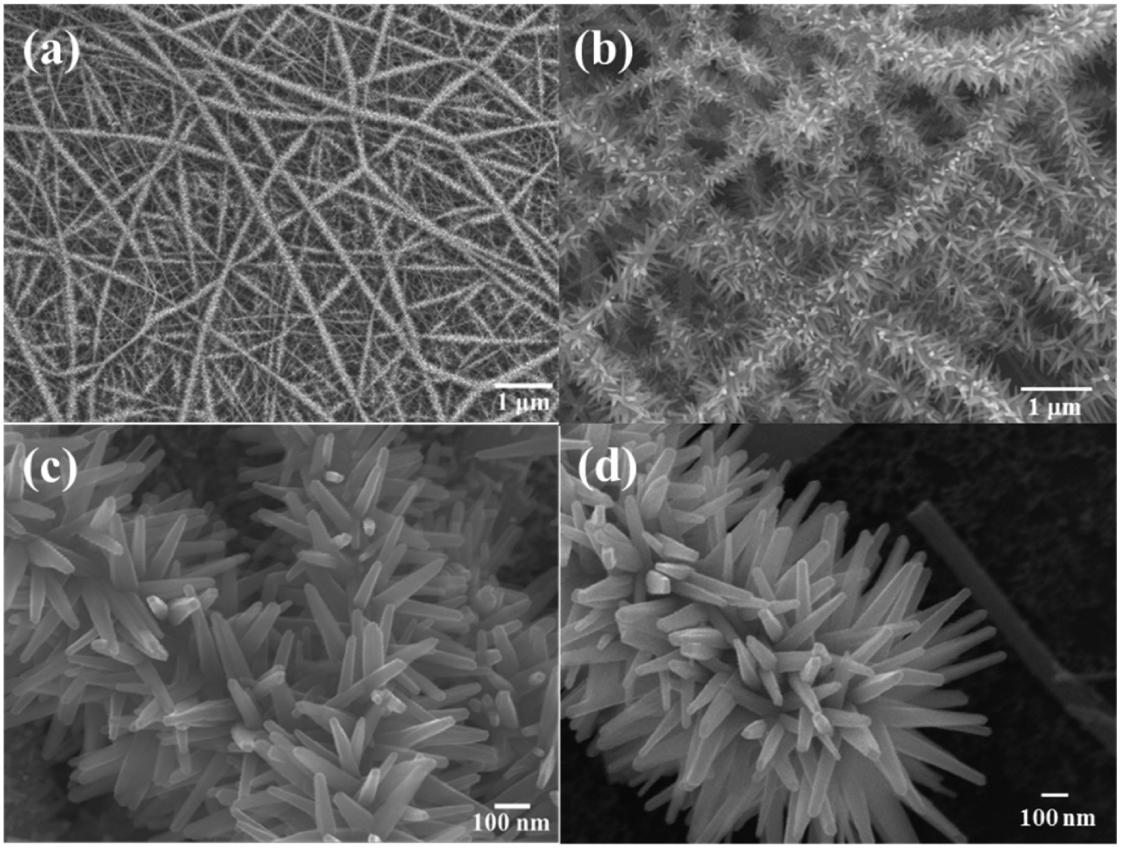

Figure 3. Low- and high-magnification SEM images of RuO_2 nanoneedles on electrospun TiO_2 nanofibers grown from a $Ru(OH)_3$ precursor solution by thermal annealing at 300 °C.

tetraisopropoxide/PVP nanofibers exhibited a fine surface morphology before being thermally annealed, and the diameter of the as-spun nanofibers was in the 300−500 nm range, as shown in Figures 2a and 2b. In contrast, the diameter of TiO_2 nanofibers was greatly reduced to mostly between 100 and 300 nm after the thermal annealing process at 500 °C in air. The surface morphology was also changed from a smooth surface to a rough surface as the matrix polymer was rapidly removed through the calcination process at 500 °C in air. During the thermal annealing process, titanium tetraisopropoxide/PVP nanofibers were converted into the connections of polycrystalline TiO_2 nanoparticles to form the nanofibers. RuO_2 nanoneedles were then grown on the TiO_2 nanofibers during thermal annealing at 300 °C for 4 h by directly spreading $Ru(OH)_3$ precursor solution onto the surface of the rough TiO_2 nanofibers. Figure 3 shows that the RuO_2 nanoneedles were well grown with a remarkably high density and that they covered the entire surface of the TiO_2 nanofibers. The RuO_2 nanoneedles on electrospun nanofibers exhibited high aspect ratios, with a lateral dimension in the 30−50 nm range and lengths ranging from ∼300 nm to ∼1000 nm. Also, the atomic % ratio of RuO_2 and TiO_2 by careful measurements in EDS is 21.6:78.4 in RuO_2 nanoneedles on electrospun TiO_2 nanofibers. However, the lateral dimension was rather tapered along the length from the root to the tip, as is typical for products of vapor−solid growth processes.[18] However, because the growth of RuO_2 was carried out at a relatively low temperature of 300 °C, where the equilibrium vapor pressure of the pure RuO_2 is negligible, the tapering of the lateral dimension cannot be attributed to this model. Rather, the growth of the nanoneedles is ascribed to the diffusion of the amorphous $Ru(OH)_3$ nanoparticles on the surface of TiO_2 nanofibers, resulting in the formation of the tip-like geometry of a single nanoneedle, where the driving force for the diffusion is related to the internal stress associated with the phase formation. At the nucleation step, amorphous $Ru(OH)_3$ nanoparticles on particle-like electrospun TiO_2 nanofibers are expected to be initially converted into anhydrous RuO_2 nanoparticles with the loss of the water of hydration; these nanoparticles then initiate the direct crystallization process. Therefore, the formation of the nanoneedles is reasonably deduced to have been achieved by continuous feedbacks of diffusing crystallized nanoparticles in the vicinity of the nucleation sites. The morphology of the grown RuO_2 nanoneedles at the tip exhibited a polyhedral or rectangular cross-section. In contrast, $Ru(OH)_3$ nanoparticles could not grow on the crystalline nanoneedles at lower temperatures (below 150 °C) and for the short annealing time, as shown in Figure S1. $Ru(OH)_3$ nanoparticles on electrospun TiO_2 nanofibers were clearly transformed into the needle shape with high crystallinity above 250 °C in air by the large part of removal of H_2O as shown in Figure S2. Although the density of RuO_2 nanoneedles is high enough at 250 °C, the growth sample of 300 °C shows relatively better performance for sensing H_2O_2 in our study as summarized in Table S1. It is partially attributed to the different crystallinity of RuO_2 nanostructures depending on the growth temperature. In contrast, the morphologies of RuO_2 nanostructures on electrospun TiO_2 nanofibers are less well-defined at the temperatures higher than 300 °C. We have thus optimized RuO_2 nanostructures by carefully considering the electro-

DOI: 10.1021/acsami.5b03178
ACS Appl. Mater. Interfaces 2015, 7, 15321−15330

chemical performance for sensing H_2O_2 at the growth temperature of 300 °C.

Figure 4 shows the XRD patterns for the RuO_2 nanoneedles−TiO_2 nanofibers and the pure TiO_2 nanofibers. The

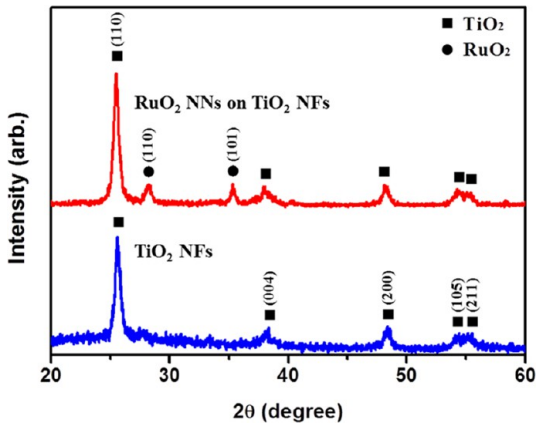

Figure 4. XRD patterns of pure TiO_2 nanofibers and RuO_2 nanoneedles on electrospun TiO_2 nanofibers.

positions of all of the pure TiO_2 nanofiber peaks at 25.4°, 37.9°, 48.2°, 54.2°, and 55.2° are very closely matched with the (110), (004), (200), (105), and (211) planes corresponding to the anatase phase (JCPDS 84-1286) of the tetragonal TiO_2 structure, quite consistent with values reported for electrospun fibers formed at 500 °C.[15] The rutile-phase TiO_2 nanofibers were not formed because the transformation from the anatase structure to the rutile structure of TiO_2 occurs at approximately 750 °C.[15] However, in the XRD pattern of RuO_2 nanoneedles on the TiO_2 nanofibers, additional peak positions at 28.1° and 35.7° clearly correspond to the (110) and (101) planes of the RuO_2 tetragonal rutile phase.[19] In addition, no evidence was observed for the partial contribution regarding a mixed crystalline phase between RuO_2 and TiO_2 (i.e., $Ru_{1-x}Ti_xO_2$). This lack of a mixed phase is likely a consequence of the growth temperature being too low for the formation of a single-phase mixed oxide.

The detailed crystal structure was carefully characterized by HRTEM, as shown in Figure 5. Figure 5a shows a low-magnification TEM image of RuO_2 nanoneedles on a single 70-nm-diameter TiO_2 nanofiber grown at 300 °C, where the lateral dimension of the TiO_2 nanofiber was approximately 25 nm. Figure 5b shows a TiO_2 nanofiber consisting of continuously connected TiO_2 particles with diameters less than 10 nm; the surface of the fiber is quite rough. The existence of many different crystalline phases in a TiO_2 nanofiber confirms the polycrystalline nature of a TiO_2 nanofiber. The SAED pattern in Figure 5c shows typical ring structures associated with the polycrystalline structure of the TiO_2 nanofibers. However, the HRTEM image and the corresponding fast Fourier transform (FFT) for a RuO_2 nanoneedle attached to a TiO_2 nanofiber reveal highly ordered lattice fringes, demonstrating that the nanowire is a defect-free single crystal (Figure 5d and Figure S3). The RuO_2 nanoneedle is identified as a tetragonal crystalline phase, and its growth occurs along the [001] direction, as evident from the FFT of the lattice-resolved image in Figure 5d. Furthermore, EDS element mapping analysis of

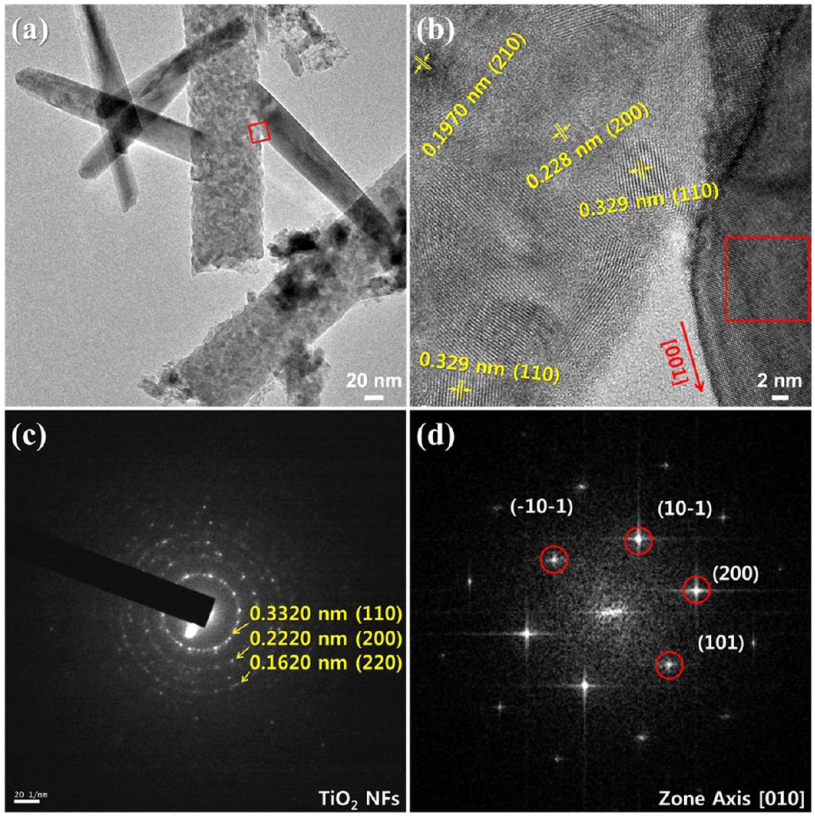

Figure 5. Low- and high-magnification TEM images of RuO_2 nanoneedles on TiO_2 nanofibers: (a) Low-resolution TEM image of RuO_2 nanoneedles and TiO_2 nanofibers; (b) HRTEM image of a single RuO_2 nanoneedle on TiO_2 nanofibers; (c) SAED pattern of a single TiO_2 nanofiber; and (d) fast Fourier transform (FFT) of the lattice-resolved image of a single RuO_2 nanoneedle.

DOI: 10.1021/acsami.5b03178
ACS Appl. Mater. Interfaces 2015, 7, 15321−15330

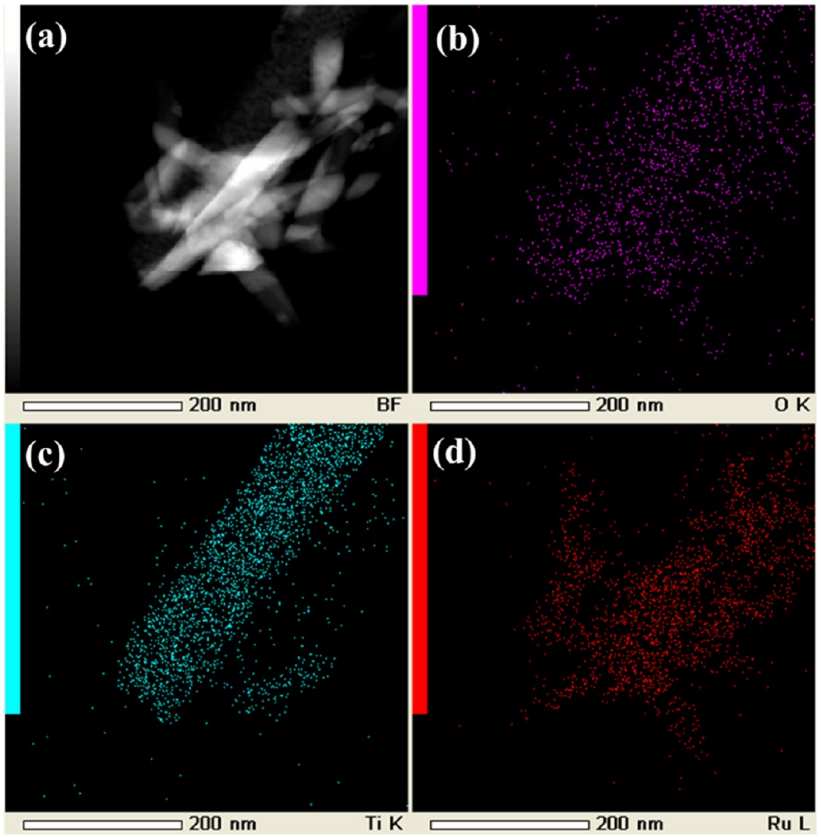

Figure 6. (a) HADDF-STEM image of RuO_2 nanoneedles on TiO_2 nanofibers and EDS mapping of elements for O (b), Ti (c), and Ru (d) in RuO_2 nanoneedles on electrospun TiO_2 nanofibers.

the material in the high-angle annular dark field (HAADF) STEM image shown in Figure 6 shows the distribution of Ti, Ru, and O, clearly demonstrating distinct regions of Ru and Ti atoms in the branched nanostructures. This result confirms that the backbone of the nanofibers consists primarily of Ti and O atoms, whereas the branch nanowires are composed of Ru and O atoms. Thus, we have successfully grown highly branched single-crystalline RuO_2 nanoneedles on TiO_2 nanofibers at a relatively low temperature using a two-step process; this process consists of a combination of an electrospinning process and a thermal annealing process from a precursor solution. This synthetic route for RuO_2 nanoneedle–TiO_2 nanofiber nanostructures exhibits several favorable features: it is simple, cost-effective, and versatile for the development of new functional platforms toward efficient electrocatalysts.

Electrochemical characterization. Figure 7 shows the CV curves of RuO_2 nanoneedles–TiO_2 nanofibers, $Ru(OH)_3$–TiO_2 nanofibers, and TiO_2 nanofibers obtained at various scan rates in a background electrolyte solution containing 1.0 M KCl. The absolute nonfaradaic capacitive current difference (Δi = |anodic i − cathodic i| at 0.35 V vs SCE) of RuO_2 nanoneedles–TiO_2 nanofibers exhibits good linear proportionality to the scan rate. High-surface-area electrode materials are important in supercapacitors or pseudocapacitors. RuO_2 and $Ru(OH)_3$ act as pseudocapacitors, contributing both double-layer and Faradaic charge, and can generate a specific capacitance as high as 720 F/g.[20] An ideal double-layer capacitor requires that the sign of the current changes immediately after the reversal of the potential and a voltammogram with a rectangular shape.[21] However, the shape of the CV curve for the $Ru(OH)_3$–TiO_2 nanofibers

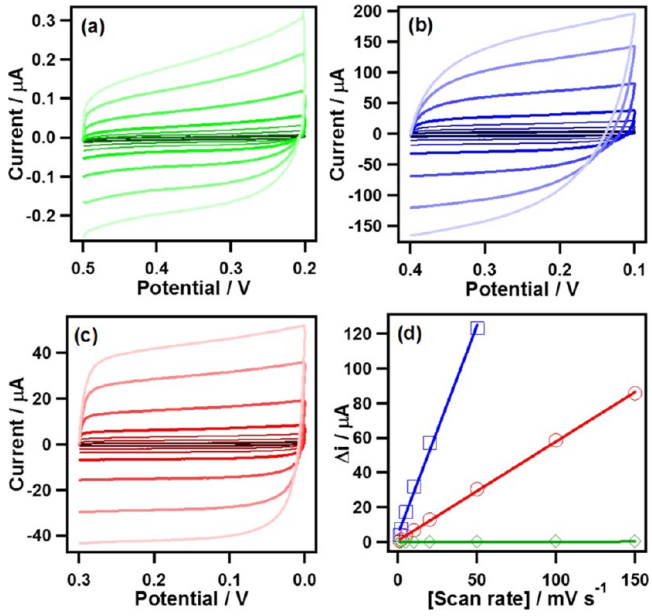

Figure 7. CVs of (a) TiO_2 nanofibers, (b) $Ru(OH)_3$–TiO_2 nanofibers, and (c) RuO_2 nanoneedles–TiO_2 nanofibers in 0.1 M KCl aqueous solution at various scan rates (1, 2, 5, 10, 20, 50, 100, and 150 mV s^{-1}). (d) Plots of the difference of capacitive current (Δi) vs scan rate: TiO_2 nanofibers (◇) at 0.35 V $Ru(OH)_3$–TiO_2 nanofibers and (□) at 0.25 V; RuO_2 nanoneedles–TiO_2 nanofibers (○) at 0.15 V.

electrode deviates significantly from rectangular; this electrode also does not exhibit good linear proportionality to the scan rate, indicating that this electrode exhibits a slow charge-

DOI: 10.1021/acsami.5b03178
ACS Appl. Mater. Interfaces 2015, 7, 15321−15330

transfer rate. The slope (Δi vs scan rate) related to the real surface area (RSA) of the electrode was measured to be 4.23 times greater for $Ru(OH)_3$–TiO_2 nanofibers than for RuO_2 nanoneedles–TiO_2 nanofibers. Given the double-layer capacitance (C_{dl}) values (80 μF cm^{-2} for RuO_2, 1403 μF cm^{-2} for $Ru(OH)_3$), this slope corresponds to a 4.15-fold increase in the electroactive RSA at the RuO_2 nanowires–TiO_2 nanofibers (7.13 cm^2) compared to the $Ru(OH)_3$–TiO_2 nanofibers (1.72 cm^2).[20,22]

The general electrochemical activities of RuO_2 nanoneedles–TiO_2 nanofibers, $Ru(OH)_3$–TiO_2 nanofibers, and TiO_2 nanofibers were examined by CV for the reduction of $[Fe(CN)_6]^{3-}$ at various scan rates. The measured cathodic currents are linearly proportional to the square root of the scan rate for all of the RuO_2 nanoneedles–TiO_2 nanofibers, $Ru(OH)_3$–TiO_2 nanofibers, and TiO_2 nanofibers (Figure 8).

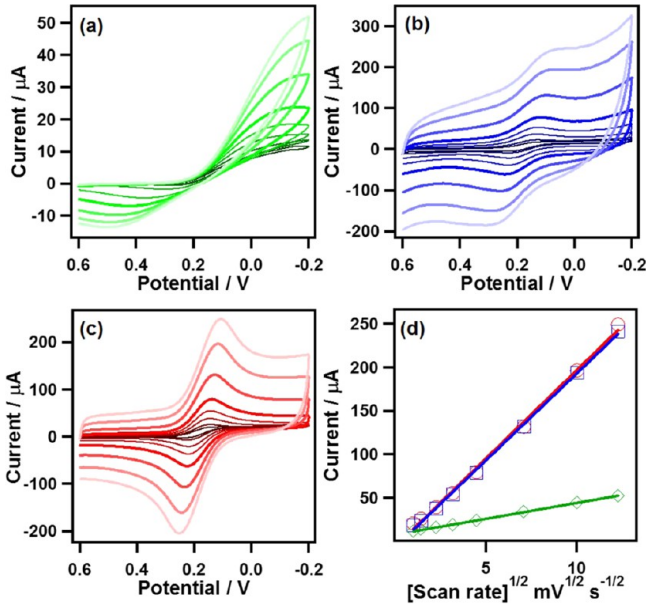

Figure 8. CVs of (a) TiO_2 nanofibers, (b) $Ru(OH)_3$–TiO_2 nanofibers and (c) RuO_2 nanowires–TiO_2 nanofibers with different scan rates (1, 2, 5, 10, 20, 50, 100, and 150 mV s^{-1}) in a solution containing 10 mM $[Fe(CN)_6]^{3-}$ and 0.1 M KCl. (d) Plots for the current peak at the reduction peak potential vs [scan rate]$^{1/2}$: TiO_2 nanofibers (◇), $Ru(OH)_3$–TiO_2 nanofibers (□), and RuO_2 nanoneedles–TiO_2 nanofibers (○).

CV curves of all the materials at rather low scan rates (1, 2, 5, 10 mV s^{-1}) can be more clearly seen in the Supporting Information (Figures S4 and S5). As reported elsewhere,[23] the reference TiO_2 nanofibers without RuO_2 nanoneedles or $Ru(OH)_3$ exhibit poor voltammetric behavior for the $[Fe(CN)_6]^{3-/4-}$ couple, indicating rather poor electric conductivity of the TiO_2 nanofibers at room temperature. In contrast, voltammetric current peaks are clearly apparent for the RuO_2 nanoneedles–TiO_2 nanofibers and $Ru(OH)_3$–TiO_2 nanofibers. This result implies that the high electroactivities of RuO_2 nanoneedles–TiO_2 nanofibers and $Ru(OH)_3$–TiO_2 nanofibers allow fast electron transfer for the $[Fe(CN)_6]^{3-/4-}$ couple. A comparison of the peak currents measured at the same scan rate reveals that RuO_2 nanoneedles–TiO_2 nanofibers and $Ru(OH)_3$–TiO_2 nanofibers show ~4.79-fold greater currents than the TiO_2 nanofibers. The slope (cathodic peak current vs scan rate$^{1/2}$) of the RuO_2 nanoneedles–TiO_2 nanofibers electrode is similar to that of the $Ru(OH)_3$-TiO_2 nanofibers electrode. This observation also supports the hypothesis that the $[Fe(CN)_6]^{3-}$ reduction at the RuO_2 nanoneedles–TiO_2 nanofibers and the $Ru(OH)_3$-TiO_2 nanofibers is a diffusion-controlled process in which the current is proportional to the geometric surface area (GSA) of the electrodes rather than to the RSA.

The electron-transfer kinetics of the $[Fe(CN)_6]^{3-/4-}$ couple at the electrode surface was also investigated by EIS at 0.139 V (vs SCE), which is the potential for the cathode peak current at the RuO_2 nanoneedles–TiO_2 nanofibers-loaded GC electrode under the same conditions used for the CV experiments. As shown in Figure 9, the Nyquist plot shows a semicircle related

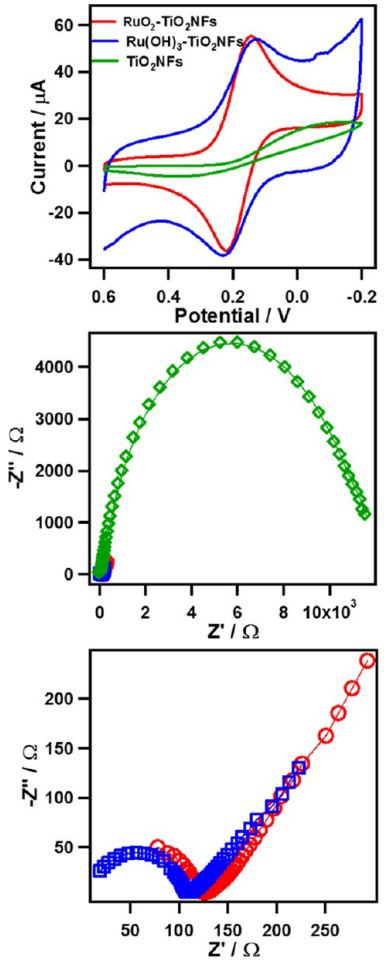

Figure 9. CVs at 10 mV s^{-1} (top) and Nyquist plots of TiO_2 nanofibers, $Ru(OH)_3$–TiO_2 nanofibers, and RuO_2 nanoneedles–TiO_2 nanofibers (middle, bottom). Nyquist plots are measured at 0.139 V, which is the potential of the cathode peak current in CV at the RuO_2 nanoneedles–TiO_2 nanofibers in the frequency range from 1 Hz to 10 kHz. The other conditions are the same as in Figure 8.

to the redox probe $[Fe(CN)_6]^{3-/4-}$ couple, followed by a Warburg line in the low-frequency region, which corresponds to the diffusion step of the overall process. The collected impedance data were then analyzed using a modified Randles circuit. The impedance of a faradaic reaction consists of an active charge-transfer resistance (R_{ct}) and a specific electrochemical element of diffusion (Z_w), also referred to as the Warburg element ($Z_w = A_w/(j\omega)^{0.5}$, where A_w is the Warburg coefficient, j is the imaginary unit, and ω is the angular frequency). The Warburg impedance is noticeable at low

DOI: 10.1021/acsami.5b03178
ACS Appl. Mater. Interfaces 2015, 7, 15321–15330

frequencies. The equivalent circuit was used mainly to determine C_{dl} and R_{ct}. Because the solution resistance (R_s) and Z_w represent the bulk properties of the electrolyte solution and the diffusion of the applied redox probe, respectively, they are not sensitive to chemical transformations at the electrode interface.[24] Thus, changes in C_{dl} should be negligible compared to changes in R_{ct}. A redox-active probe is useful in this case, resulting in a well-defined R_{ct}. The R_{ct} values of the RuO_2 nanoneedles−TiO_2 nanofibers electrode (~120 Ω) and the $Ru(OH)_3$−TiO_2 nanofibers electrode (~110 Ω) were significantly smaller than those of the TiO_2 nanofibers electrode (~1.2×10^4 Ω), corroborating the CV results in Figure 9.

Electrocatalysis of H_2O_2 at RuO_2 nanoneedles−TiO_2 nanofibers. Electrochemical oxidation and reduction of a biological species, H_2O_2, were investigated by RDE voltammetry at GC electrodes loaded with RuO_2 nanoneedles−TiO_2 nanofibers, $Ru(OH)_3$−TiO_2 nanofibers, and TiO_2 nanofibers. As shown in Figure 10a, H_2O_2 oxidation and reduction occurred at all of the electrodes loaded with RuO_2 nanoneedles−TiO_2 nanofibers, $Ru(OH)_3$−TiO_2 nanofibers, and TiO_2 nanofibers within the experimental potential scan range (−0.2 to 0.7 V vs SCE) at 100 rpm. The anodic current at RuO_2 nanoneedles−TiO_2 nanofibers was initially observed at ~0.23 V and increased significantly as the potential moved in the positive direction during the course of the RDE measurement. The onset potential for H_2O_2 oxidation for RuO_2 nanoneedles−TiO_2 nanofibers was more negative than that for $Ru(OH)_3$−TiO_2 nanofibers. The RuO_2 nanoneedes−TiO_2 nanofibers also exhibit catalytic activity for H_2O_2 reduction, as indicated by the observed cathodic current for potentials lower than 0.23 V, although this activity is relatively small compared to that toward H_2O_2 oxidation. Notably, the oxidations and reductions of H_2O_2 were observed for both RuO_2 nanoneedles−TiO_2 nanofibers and $Ru(OH)_3$−TiO_2 nanofibers, but RuO_2 nanoneedles−TiO_2 nanofibers generated a greater limiting current in the RDE curve.

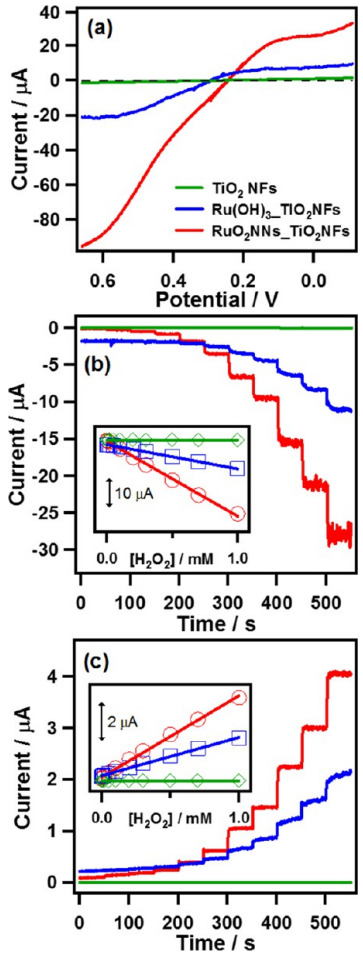

Figure 10. (a) Background-corrected RDE curves of TiO_2 nanofibers, $Ru(OH)_3$−TiO_2 nanofibers and RuO_2 nanoneedles−TiO_2 nanofibers obtained in 0.05 phosphate buffer solution containing 5.0 mM H_2O_2 at a scan rate of 5 mV s^{-1}. (b, c) Dynamic current responses of TiO_2 nanofibers, $Ru(OH)_3$−TiO_2 nanofibers, and RuO_2 nanoneedles−TiO_2 nanofibers to an increase of the H_2O_2 concentration in 0.05 M phosphate buffer solution. Electrode potential: (b) 0.6 V vs SCE for H_2O_2 oxidation and (c) 0.0 V vs SCE for H_2O_2 reduction. Insets of (b) and (c) show the corresponding calibration plots.

According to the RDE results shown in Figure 10a, 0.60 V (vs SCE) for H_2O_2 oxidation and 0.0 V (vs SCE) for H_2O_2 reduction, which were measured for the oxidations and reductions of H_2O_2 at all of the investigated electrodes, were chosen as the applied electrode potentials for monitoring the amperometric response to H_2O_2. Figure 10b shows the typical dynamic current response curves to H_2O_2 concentration and the corresponding calibration curves for H_2O_2 oxidation at 0.60 V. Moreover, as observed in Figure 10c, the measured cathodic current also increased as the H_2O_2 concentration increased. The current changed faster in response to the variation in H_2O_2 concentration at the RuO_2 nanoneedles−TiO_2 nanofibers electrode than at the $Ru(OH)_3$-TiO_2 nanofibers electrode: the response times ($t_{95\%}$, time to reach 95% of the steady-state electrode current) of the RuO_2 nanoneedles−TiO_2 nanofibers were estimated to be 3.57 ± 0.77 s (n = 5) for H_2O_2 oxidation and 2.53 ± 0.93 s (n = 5) for H_2O_2 reduction on the basis of the typical dynamic current response curves. By comparison, the $t_{95\%}$ values of the $Ru(OH)_3$−TiO_2 nanofibers were estimated to be 10.1 ± 7.3 s (n = 5) for H_2O_2 oxidation and 10.7 ± 3.8 s (n = 5) for H_2O_2 reduction.

The calibration plots corresponding to the amperometric current response measurements are presented in the insets of Figures 10b and 10c. These plots show a highly linear relationship between the measured currents and the H_2O_2 concentration for the tested concentration range (1 to 1000 μM) at both the RuO_2 nanoneedles−TiO_2 nanofibers and the $Ru(OH)_3$−TiO_2 nanofibers. The GC electrode loaded with RuO_2 nanoneedles−TiO_2 nanofibers exhibited 3-fold greater sensitivities (−29.0 μA mM^{-1}, R^2 = 0.998 for H_2O_2 oxidation; 3.96 μA mM^{-1}, R^2 = 0.998 for H_2O_2 reduction) compared to the electrodes loaded with $Ru(OH)_3$−TiO_2 nanofibers and TiO_2 nanofibers (−9.40 μA mM^{-1}, R^2 = 0.999 for H_2O_2 oxidation; 1.86 μA mM^{-1}, R^2 = 0.998 for H_2O_2 reduction), suggesting that the RuO_2 nanoneedles−TiO_2 nanofibers are potentially good H_2O_2 sensing materials. The sensitivities at electrodes loaded with RuO_2 nanoneedles−TiO_2 nanofibers were measured to be −27.7 ± 1.1 μA mM^{-1} for H_2O_2 oxidation and 3.82 ± 0.08 μA mM^{-1} for H_2O_2 reduction for five different electrodes. The relatively small standard deviation of the sensitivity indicates the high reproducibility of this RuO_2 nanoneedles−TiO_2 nanofibers-loaded GC electrode. The detection limit was determined to be 0.001 mM at a signal-to-noise ratio of 3. These electrochemical performances of the RuO_2 nanoneedles−TiO_2 nanofibers grown at 300 °C are relatively better than those of the sample grown at 250 °C due to the higher crystallinity of RuO_2 nanostructures as shown in

DOI: 10.1021/acsami.5b03178
ACS Appl. Mater. Interfaces 2015, 7, 15321−15330

Table 1. Comparison of Analytical Performances of Reported Amperometric H_2O_2 Sensor vs Current Work

ref	Electrodes	Solutions	Electrode Potential[a]/V	Sensitivity[b] /μA mM^{-1} cm^{-2}	Linear Range/ μM	Detection Limit/μM	$t_{95\%}$/s
This work	RuO_2 nanoneedles−TiO_2 nanofibers	0.05 M PBS (pH 7.4)	E_{oxi} = 0.60	390.1 ± 14.9 for oxidation[c]	1−1000	1.0	3.57 ± 0.77
			E_{red} = 0.0	53.8 ± 1.1 for reduction[d]			2.53 ± 0.93
25	Co_3O_4/MWCNTs[e]	0.1 M NaOH	E_{oxi} = 0.15	729 for oxidation[c]	20−430	4.87	
			E_{red} = −0.23	1000 for reduction[d]		2.46	
26	$Ni(OH)_2$/ERGO−MWNT/GCE[f]	0.1 M NaOH	E_{oxi} = 0.15	717[c]	10−9050	4.0	2.0
27	CdO/MWCNTs[g]	PBS (pH 7.0)	E_{red} = −1.2	6147[d]	5−200	0.1	
28	PtIr/C[h]	0.1 M PBS (pH 7.0)	E_{oxi} = 0.25	49.66[c]	0−1000		
				14.40[c]	2000−10000		
29	Cu/PSi-CPE[i]	0.1 M PBS (pH 7.0)	E_{red} = −0.15	184.4[d]	0−3780	0.27	
30	TiO_2/Au/GC[j]	0.1 M PBS (pH 7.4)	E_{oxi} = 0.77	664[c]	1−7000	0.1	3
7	RuO_2 nanorods-CF[k]	0.05 M PBS (pH 7.4)	E_{oxi} = 0.50	1560 ± 103[c]	180−2620	2.3	

[a]Recalculated vs SCE. [b]Normalized to electrode geometric surface area. [c]Sensitivity for oxidation. [d]Sensitivity for reduction. [e]Cobalt(II) dicobalt(III) oxide nanoparticles anchored to multiwalled carbon nanotubes. [f]$Ni(OH)_2$ nanoparticles on an electroreduced graphene oxide-multiwalled carbon nanotube nanocomposite film modified glassy carbon electrode. [g]Cadmium oxide/multiwalled carbon nanotubes. [h]Carbon supported platinum−iridium bimetallic nanoparticles. [i]Copper on porous silicon nanocomposite-based carbon paste electrode. [j]Au/TiO_2 nanofilm-modified glassy carbon electrode. [k]Single crystalline RuO_2 nanorods grown on a single carbon fiber.

Table S1. The analytical performance of the RuO_2 nanoneedles−TiO_2 nanofibers for H_2O_2 detection was compared with the performance of recently reported electrochemical H_2O_2 sensors, as presented in Table 1. The RuO_2 nanoneedles−TiO_2 nanofibers exhibited a high sensitivity, a low detection limit, and a wide linear range, indicating better or comparable H_2O_2 detection performance compared to those of the other sensing systems.

Generally, the electrochemical oxidation and reduction of H_2O_2 is known to be a relatively sluggish process. In the case of electrode reactions with slow heterogeneous electron transfer rates just like H_2O_2 redox reactions, the large real surface area of electrode materials is the main factor to enhance the sensitivity of the amperometric measurements. As we described in the Introduction, RuO_2 is generally known as good a electrocatalytic material with high electrical conductivity. Meanwhile, TiO_2 does not have good electrical conductivity, as shown in the CV results. Consequently, the role of TiO_2 in RuO_2 nanoneedles−TiO_2 nanofibers is a skeletal backbone of this structure and provides favorable growing sites for single crystalline RuO_2 nanoneedles. Therefore, the significantly enlarged surface area of RuO_2 nanoneedles−TiO_2 nanofibers, and also the excellent conductivity of the RuO_2 material itself, could synergistically contribute to the high detection performance for H_2O_2.

CONCLUSIONS

We have successfully grown highly branched single-crystalline RuO_2 nanoneedles on polycrystalline electrospun TiO_2 nanofibers at a relatively low temperature using a two-step process consisting of a combination of an electrospinning process and a thermal annealing process from a precursor solution; the new process is simple and cost-effective and exhibits the versatility necessary for the development of a new functional platform for efficient electrocatalysts. The key feature is single-crystalline RuO_2 nanoneedles with relatively small dimensions (30−50 nm) and a high density on the electrospun TiO_2 nanofibers. The general electrochemical activities of the RuO_2 nanoneedles−TiO_2 nanofibers and $Ru(OH)_3$−TiO_2 nanofibers were carefully examined by CV for the reduction of $[Fe(CN)_6]^{3-}$ at various scan rates; they exhibited favorable charge-transfer kinetics for $[Fe(CN)_6]^{3-}$ reduction via a diffusion-controlled process. Additionally, a test of the analytical performance of the RuO_2 nanoneedles−TiO_2 nanofibers for the detection of a biologically important molecule, H_2O_2, showed high sensitivity (390.1 ± 14.9 μA mM^{-1} cm^{-2} for H_2O_2 oxidation and 53.8 ± 1.1 μA mM^{-1} cm^{-2} for reduction), a low detection limit (1 μM), and a wide linear range (1−1000 μM); these results indicate that the H_2O_2 detection performance of these electrodes is better or comparable to that of other sensing systems.

ASSOCIATED CONTENT

Supporting Information

Additional SEM images and HRTEM images for highly branched RuO_2 nanoneedles on electrospun TiO_2 nanofibers and additional electrochemical performance experiments. The Supporting Information is available free of charge on the ACS Publications website at DOI: 10.1021/acsami.5b03178.

AUTHOR INFORMATION

Corresponding Authors

*(Y.L.) E-mail: youngmilee@ewha.ac.kr.
*(M.H.K.) E-mail: myungkim@ewha.ac.kr.

Author Contributions

‖S.K. and Y.K.C. contributed equally to this work.

Notes

The authors declare no competing financial interest.

ACKNOWLEDGMENTS

This work was financially supported by the DGIST R&D Program of the Ministry of Science, ICT and Future Planning of Korea (14-BD-01); the National Research Foundation of Korea (NRF), funded by the Ministry of Science, ICT and Future Planning (2014R1A2A2A05003769 for Y.L.); and the

DOI: 10.1021/acsami.5b03178
ACS Appl. Mater. Interfaces 2015, 7, 15321−15330

National Research Foundation of Korea (NRF), funded by the Korean Government (2014R1A1A2059791 for M.H.K.).

REFERENCES

(1) Over, H. Surface Chemistry of Ruthenium Dioxide in Heterogeneous Catalysis and Electrocatalysis: From Fundamental to Applied Research. *Chem. Rev.* **2012**, *112*, 3356−3426.
(2) Wang, C. X.; Osada, M.; Ebina, Y.; Li, B. W.; Akatsuka, K.; Fukuda, K.; Sugimoto, W.; Ma, R. Z.; Sasaki, T. All-Nanosheet Ultrathin Capacitors Assembled Layer-by-Layer via Solution-Based Processes. *ACS Nano* **2014**, *8*, 2658−2666.
(3) Zhang, C. F.; Xie, Y. B.; Zhao, M. Q.; Pentecost, A. E.; Ling, Z.; Wang, J. T.; Long, D. H.; Ling, L. C.; Qiao, W. M. Enhanced Electrochemical Performance of Hydrous RuO_2/Mesoporous Carbon Nanocomposites via Nitrogen Doping. *ACS Appl. Mater. Interfaces* **2014**, *6*, 9751−9759.
(4) Gorski, W.; Aspinwall, C. A.; Lakey, J. R. T.; Kennedy, R. T. Ruthenium catalyst for amperometric determination of insulin at physiological pH. *J. Electroanal. Chem.* **1997**, *425*, 191−199.
(5) Jiang, J. C.; Zhang, W. D. Electroanalysis of Dopamine at RuO_2 Modified Vertically Aligned Carbon Nanotube Electrode. *Electroanalysis* **2009**, *21*, 1811−1815.
(6) Allen, B. W.; Piantadosi, C. A. Electrochemical activation of electrodes for amperometric detection of nitric oxide. *Nitric Oxide* **2003**, *8*, 243−252.
(7) Kang, M.; Lee, Y.; Jung, H.; Shim, J. H.; Lee, N.-S.; Baik, J. M.; Lee, S. C.; Lee, C.; Lee, Y.; Kim, M. H. Single Carbon Fiber Decorated with RuO_2 Nanorods as a Highly Electrocatalytic Sensing Element. *Anal. Chem.* **2012**, *84*, 9485−9491.
(8) Kim, S.; Jung, H.; Lee, C.; Kim, M. H.; Lee, Y. Biological application of RuO_2 nanorods grown on a single carbon fiber for the real-time direct nitric oxide sensing. *Sens. Actuators, B* **2014**, *191*, 298−304.
(9) Qiu, B. C.; Xing, M. Y.; Zhang, J. L. Mesoporous TiO_2 Nanocrystals Grown in Situ on Graphene Aerogels for High Photocatalysis and Lithium-Ion Batteries. *J. Am. Chem. Soc.* **2014**, *136*, 5852−5855.
(10) Johnson, J. M.; Kinsinger, N.; Sun, C. H.; Li, D. S.; Kisailus, D. Urease-Mediated Room-Temperature Synthesis of Nanocrystalline Titanium Dioxide. *J. Am. Chem. Soc.* **2012**, *134*, 13974−13977.
(11) Liu, H. Y.; Joo, J. B.; Dahl, M.; Fu, L. S.; Zeng, Z. Z.; Yin, Y. D. Crystallinity control of TiO_2 hollow shells through resin-protected calcination for enhanced photocatalytic activity. *Energy Environ. Sci.* **2015**, *8*, 286−296.
(12) Ma, T. L.; Akiyama, M.; Abe, E. High-efficiency dye-sensitized solar cell based on a nitrogen-doped nanostructured titania electrode. *Nano Lett.* **2005**, *5*, 2543−2547.
(13) Lee, W. S.; Park, Y. S.; Cho, Y. K. Hierarchically Structured Suspended TiO_2 Nanofibers for Use in UV and pH Sensor Devices. *ACS Appl. Mater. Interfaces* **2014**, *6*, 12189−12195.
(14) Zhang, N. A.; Deng, Y. L.; Tai, Q. D.; Cheng, B. R.; Zhao, L. B.; Shen, Q. L.; He, R. X.; Hong, L. Y.; Liu, W.; Guo, S. S. Electrospun TiO_2 Nanofiber-Based Cell Capture Assay for Detecting Circulating Tumor Cells from Colorectal and Gastric Cancer Patients. *Adv. Mater.* **2012**, *24*, 2756−2760.
(15) Li, D.; Xia, Y. Fabrication of Titania Nanofibers by Electrospinning. *Nano Lett.* **2003**, *3*, 555−560.
(16) Greiner, A.; Wendorff, J. H. Electrospinning:A Fascinating Method for the Preparation of Ultrathin Fibers. *Angew. Chem., Int. Ed.* **2007**, *46*, 5670−5673.
(17) Lee, J.; Yang, H. S.; Lee, N. S.; Kwon, O.; Shin, H. Y.; Yoon, S.; Baik, J. M.; Seo, Y. S.; Kim, M. H. Hierarchically assembled 1-dimensional hetero-nanostructures: single crystalline RuO_2 nanowires on electrospun IrO_2 nanofibres. *CrystEngComm* **2013**, *15*, 2367−2371.
(18) Pan, Z. W.; Dai, Z. R.; Wang, Z. L. Nanobelts od semiconducting oxides. *Science* **2001**, *291*, 1947−1949.
(19) Lee, Y.; Ye, B. U.; Yu, H. K.; Lee, J. L.; Kim, M. H.; Baik, J. M. Facile Synthesis of Single Crystalline Metallic RuO_2 Nanowires and Electromigration-Induced Transport Properties. *J. Phys. Chem. C* **2011**, *115*, 4611−4615.
(20) Zheng, J. P.; Cygan, P. J.; Jow, T. R. Hydrous Ruthenium Oxide as an Electrode Material for Electrochemical Capacitors. *J. Electrochem. Soc.* **1995**, *142*, 2699−2703.
(21) Frackowiak, E.; Béguin, F. Carbon Materials for the Electrochemical Storage of Energy in Capacitors. *Carbon* **2001**, *39*, 937−950.
(22) Sugimoto, W.; Kizaki, T.; Yokoshima, K.; Murakami, Y.; Takasu, Y. Evaluation of the Pseudocapacitance in RuO_2 with a RuO_2/GC Thin Film Electrode. *Electrochim. Acta* **2004**, *49*, 313−320.
(23) Earle, M. D. The Electrical Conductivity of Titanium Dioxide. *Phys. Rev.* **1942**, *61*, 56−62.
(24) Wang, B. J.; Luo, L. Q.; Ding, Y. P.; Zhao, D. S.; Zhang, Q. L. Synthesis of Hollow Copper Oxide by Electrospinning and Its Application as a Nonenzymatic Hydrogen Peroxide Sensor. *Colloids Surf., B* **2012**, *97*, 51−56.
(25) Heli, H.; Pishahang, J. Cobalt Oxide nanoparticles Anchored to Multiwalled Carbon Nanotubes: Synthesis and Application for Enhanced Electrocatalytic Reaction and Highly Sensitive Non-enzymatic Detection of Hydrogen Peroxide. *Electrochim. Acta* **2014**, *123*, 518−526.
(26) Gao, W.; Tjiu, W. W.; Wei, J.; Liu, T. Highly Sensitive Nonenzymatic Glucose and H_2O_2 Sensor Based on $Ni(OH)_2$/electroreduced Graphene Oxide-Multiwalled Carbon Nanotube Film Modified Glass Carbon Electrode. *Talanta* **2014**, *120*, 484−490.
(27) Butwong, N.; Zhou, L.; Ng-eontae, W.; Burakham, R.; Moore, E.; Srijaranai, S.; Luong, J. H.T.; Glennon, J. D. A Sensitive Nonenzymatic Hydrogen Peroxide Sensor Using Cadmium Oxide Nanoparticles/Multiwall Carbon Nanotube Modified Glassy Carbon Electrode. *J. Electroanal. Chem.* **2014**, *717*−*718*, 41−46.
(28) Chang, S.-H.; Yeh, M.-H.; Rick, J.; Su, W.-N.; Liu, D.-G.; Lee, J.-F.; Liu, C.-C.; Hwang, B.-J. Bimetallic Catalyst of PtIr Nanoparticles with High Electrocatalytic Ability for Hydrogen Peroxide Oxidation. *Sens. Actuators, B* **2014**, *190*, 55−60.
(29) Ensafi, A. A.; Abarghoui, M. M.; Rezaei, B. Electrochimical Determination of Hydrogen Peroxide Using Copper/Porous Silicon Based Non-Enzymatic Sensor. *Sens. Actuators, B* **2014**, *196*, 398−405.
(30) Yin, X.; Guo, M.; Xia, Y.; Huang, W.; Li, Z. Amperometric Sensing of Hydrogen Peroxide on a Modified Electrode with Layered Au/TiO_2 Nanofilms from Self-Assembly at Air/Water Interface. *J. Electroanal. Chem.* **2014**, *720*−*721*, 19−23.

DOI: 10.1021/acsami.5b03178
ACS Appl. Mater. Interfaces 2015, 7, 15321−15330